Available online at www.sciencedirect.com
ScienceDirect
Journal of Solid State Chemistry 180 (2007) 1863–1874
JOURNAL OF SOLID STATE CHEMISTRY
www.elsevier.com/locate/jssc

Magnesium doping on brownmillerite Ca_2FeAlO_5

J. Malveiro[a], T. Ramos[a], L.P. Ferreira[b], J.C. Waerenborgh[c], M.R. Nunes[d], M. Godinho[e], M.D. Carvalho[d,*]

[a]*CCMM, Faculdade de Ciências, Universidade de Lisboa, 1749-016 Lisboa, Portugal*
[b]*CFMC-UL, Faculdade de Ciências, Universidade de Lisboa, 1749-016 Lisboa; Dep. Física, Faculdade de Ciências e Tecnologia, Universidade de Coimbra, 3004-516 Coimbra, Portugal*
[c]*Dep. Química, ITN/CFMC-UL, Estrada Nacional 10, P-2686-953 Sacavém, Portugal*
[d]*CCMM/Dep. Química e Bioquímica, Faculdade de Ciências, Universidade de Lisboa, Campo Grande, C8, 1749-016 Lisboa, Portugal*
[e]*CFMC-UL/Dep. Física, Faculdade de Ciências, Universidade de Lisboa, 1749-016 Lisboa, Portugal*

Received 31 January 2007; received in revised form 10 April 2007; accepted 12 April 2007
Available online 19 April 2007

Abstract

$Ca_2FeAl_{1-x}Mg_xO_5$ ($x = 0$, 0.05 and 0.1) compounds adopting the brownmillerite-type structure were prepared by a self-combustion route using two different fuels. Characterisation was performed using X-ray powder diffraction, Mössbauer spectroscopy, magnetisation measurements, chemical analysis, scanning electron microscopy and 4-point dc conductivity measurements. Global results indicate that the solubility limit was reached for $x = 0.1$. An antiferromagnetic behaviour was detected for all studied compositions, with magnetic ordering temperatures of 340 and 290 K for $x = 0$ and 0.05, respectively. Mg doping increases the number of iron cations in tetrahedral sites, which induces magnetisation enhancement at low temperatures through the coupling between octahedral iron cations in different octahedral planes. The compounds exhibit semiconductor behaviour and Mg^{2+} doping yields a significant enhancement of the total conductivity, which can be essentially attributed to the presence of Fe^{4+} ions.

Keywords: Brownmillerite; Self-combustion synthesis; Mössbauer spectroscopy

1. Introduction

Materials based on oxygen-deficient perovskite-related compounds have been attracting a great deal of interest over the past decades. Possible applications for this type of materials include fuel cells and dense membranes for the partial oxidation of hydrocarbons, where materials properties are crucial and greatly influenced by compositional homogeneity and morphology.

Amongst the many available routes to synthesise solid inorganic materials [1], the conventional solid-state route experienced widespread use until recent years, mainly because of its simplicity. However, due to the impendent necessity to obtain materials with homogeneous phase composition, fine particle size and high specific surface area, chemical approaches have been developed to ensure molecular level mixing of the multi-component mixture, with sol–gel [2,3] and combustion methods [4] being amongst the most widely used.

One of the most stable variants of oxygen vacancy ordering in the perovskites is the brownmillerite-type structure ($A_2B_2O_5$), consisting of alternating layers of corner-sharing BO_6 octahedra and BO_4 tetrahedra. Depending on the synthesis route and B cation, these compounds usually crystallise in one of the following space group symmetries: *Ibm*2, *Icmm* or *Pnma*, with *Ibm*2 and *Pnma* describing fully ordered structures, in terms of cation and oxygen displacements in the tetrahedral chains [5,6]. Structural stabilisation can be achieved when part of the B sites are occupied by cations with preference for tetrahedral coordination, such as Ga and Al [7]. If a certain degree of disorder can be introduced, brownmillerite compounds are candidates to exhibit suitable mixed-conduction. In fact, the mixed conduction characteristics of brownmillerite materials are already being exploited [8].

*Corresponding author. Fax: +351 217500088.
E-mail address: mdcarvalho@fc.ul.pt (M.D. Carvalho).

0022-4596/$ - see front matter © 2007 Elsevier Inc. All rights reserved.
doi:10.1016/j.jssc.2007.04.009

While gallium and aluminium prefer tetrahedral coordination, other metal cations are known to prefer octahedral sites. Magnesium, for instance, is well known to have a higher octahedral site preference than Fe^{3+} in spinel oxides. The same Mg/Fe site preference was suggested for a brownmillerite compound with the composition $Ca_2Fe_{0.95}Al_{0.95}Mg_{0.05}Si_{0.05}O_5$ [9]. Furthermore in the proposed compositions, the substitution of Al^{3+} ions with stable divalent Mg^{2+} should increase the amount of Fe^{4+} due to charge compensation, which can lead to significant changes in the electrical properties.

This work reports the synthesis, using two different routes (urea and citrate), of $Ca_2FeAl_{1-x}Mg_xO_5$ ($x = 0$, 0.05 and 0.1) phases and assesses, using room temperature X-ray diffraction (XRD), Mössbauer spectroscopy, magnetisation and 4-point dc conductivity measurements, the influence of both Mg^{2+} doping and synthesis route on relevant structural and compositional features and their influence on the electrical properties of these materials.

2. Experimental

Ceramic powders of $Ca_2FeAl_{1-x}Mg_xO_5$ ($x = 0$, 0.05 and 0.1) were prepared by a self-combustion route using two different fuels: citrate acid and urea. The starting metals, metal carbonates or oxalates of reagent grade were mixed and dissolved in nitric acid, in the appropriate molar ratios, for both routes. The obtained solutions were then mixed with urea or with citric acid, and heated up until a concentrated gel was formed, followed by autocombustion. The resulting powders were calcined at 873 K for 8 h, to remove any remaining organics, before being further calcined in air at temperatures ranging from 1273 to 1553 or 1573 K depending on the sample, with intermediate grinding. The synthesis process was closely monitored by XRD.

Structural characterisation by XRD was performed using a Philips PW 1730 powder diffractometer, operating with a Cu$K\alpha$ radiation and previously calibrated using a Si standard. The XRD patterns were collected within the 2θ range 10–120° with a step length of 0.02° and analysed by Rietveld refinement using the FullProf program [10]. A polynomial function was used to model the background level. Peak shapes were fitted using a pseudo-Voigt function and two asymmetry parameters. A preferred orientation correction was included in the different refinements and the total occupation factors were fixed taking into account sample stoichiometry and assuming fully occupied oxygen sites. In order to compare the results obtained for the different samples, and avoid some problems resulting from oxygen atomic displacement factors refining to unreasonable values, the atomic isotropic temperature factors were fixed at 0.01 $Å^2$, and only the overall isotropic displacement factor was refined. The refinements were performed between 15° and 120° for all cases, and a very small peak (maximum relative intensity of 0.3%) around 30°, not identified, was excluded from the refinements.

Mohr's salt titrations were performed to determine the Fe^{4+} amount for each composition.

Electrical conductivity measurements were carried out using a home-made 4-point dc conductivity apparatus at temperatures ranging from around 323 to 873 K in air. Scanning electron microscopy (SEM) images of the pellets used for the electrical conductivity measurements were obtained on a JEOL–JSM 35C microscope, operating at 20 kV.

The Mössbauer spectra were collected at room temperature, 50 and 4 K in transmission mode using a conventional constant-acceleration spectrometer and a 25 mCi ^{57}Co source in a Rh matrix. The low-temperature measurements were performed using a liquid-helium flow cryostat with a temperature stability of ± 0.5 K. Above room temperature Mössbauer spectra were obtained using a Wissel MBF-1100 furnace. The velocity scale was calibrated using an α-Fe foil. The spectra were fitted to Lorentzian lines using a non-linear least-squares method [11].

Magnetisation measurements as a function of temperature, $M(T)$, and applied magnetic field, $M(H)$, were performed using a SQUID magnetometer (Quantum Design MPMS). The $M(T)$ curves were obtained at 5 and 50 mT for temperatures ranging from 2 to 360 K. Data were collected in increasing temperature after both zero-field cooling (ZFC) and field cooling (FC). The isothermal $M(H)$ curves and hysteresis loops were measured for magnetic fields up to 5.5 T.

3. Results and discussion

3.1. XRD characterisation

The synthesis evolution was monitored by XRD, which indicated different developments depending on the method (citrate and urea). In order to compare both preparation routes, Fig. 1 shows the evolution of the XRD patterns of the $x = 0.05$ compounds, obtained after the decomposition at 873 K (8 h) and after the first thermal treatment at 1553 K (24 h), for both synthesis methods. The differences exhibited by the products after the first thermal treatment are significant. While the urea route led to a reasonably good crystalline precursor presenting a pattern similar to the desired brownmillerite phase, the precursor obtained by the citrate route is less crystalline and the observed peaks are essentially due to $CaCO_3$ and some Al_2O_3. However, after the first thermal treatment at 1553 K (24 h), a well-crystallised brownmillerite structure could be assigned for both cases.

Both $x = 0$ and 0.05 compounds were successfully synthesised by both methods at 1553 K, as the XRD patterns are consistent with the brownmillerite structure. In the case of the $x = 0.1$ compounds, the temperature treatment was increased until 1573 K in an attempt to obtained a pure phase. However, the patterns (urea and citrate) still exhibited a small extra peak (around 1% of the highest peak of the brownmillerite phase) which could be

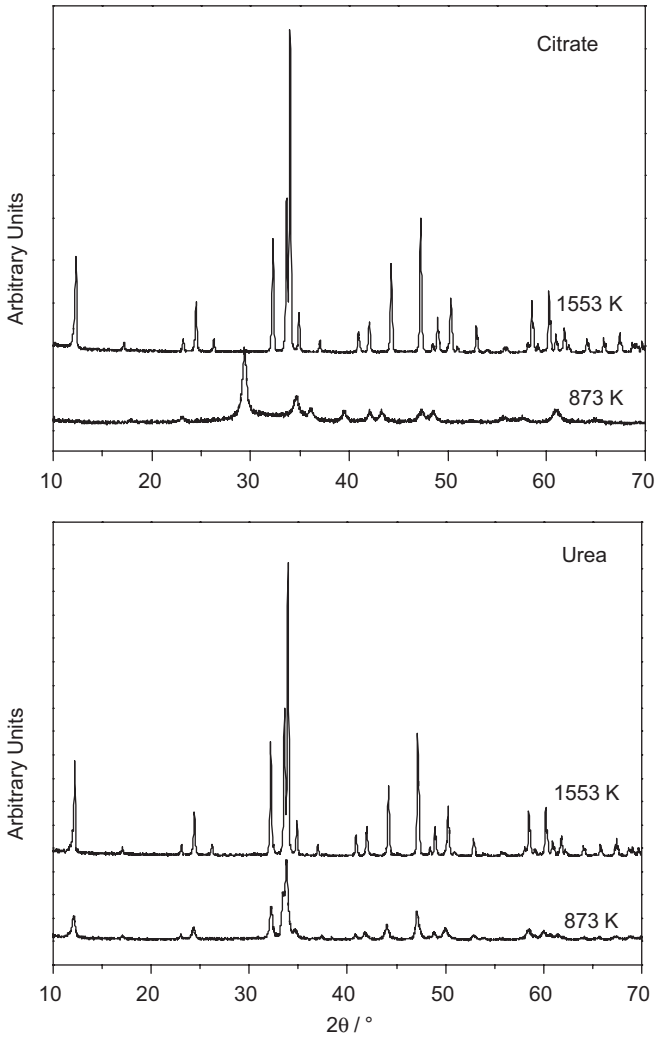

Fig. 1. Evolution of XRD patterns, for nominal composition $Ca_2FeAl_{0.95}Mg_{0.05}O_5$, for the two different synthesis routes. The patterns shown were obtained after the first thermal treatments at each indicated temperature (8 h at 873 K and 24 h at 1553 K).

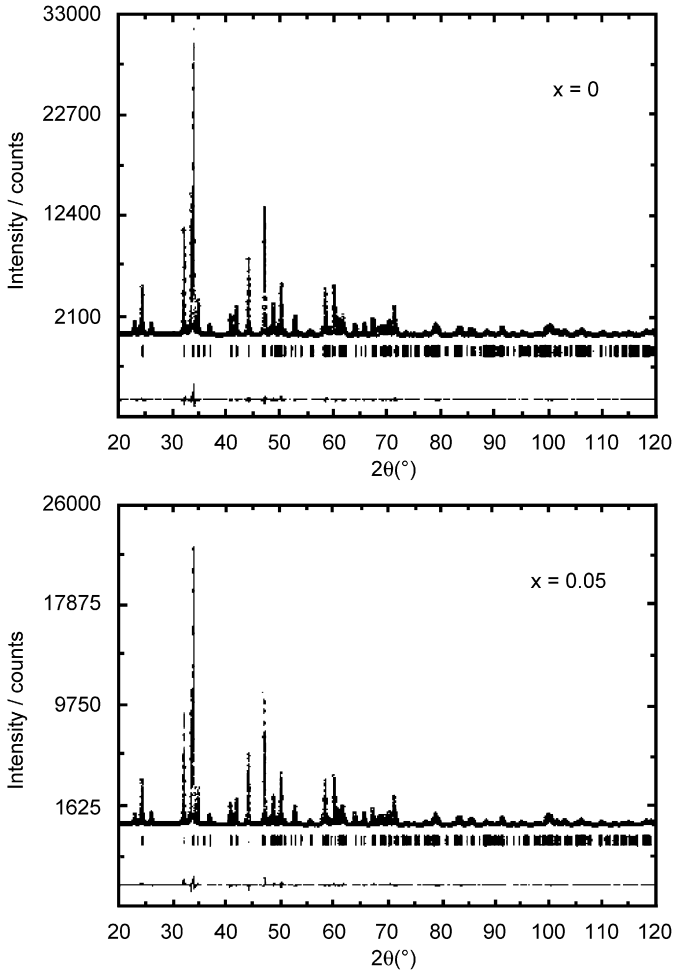

Fig. 2. Observed (points) and calculated (solid line) Rietveld refinement plots of the XRD patterns of the $Ca_2FeAl_{1-x}Mg_xO_5$ with $x = 0$ and 0.05 phases (urea route). The difference between observed and calculated is shown at the bottom of each pattern. Tick marks represent allowed reflections.

attributed to MgO, indicating that magnesium solubility was reached.

The lattice parameters and unit cell volume were obtained from the performed Rietveld refinements. For the Ca_2FeAlO_5 compound, the *Ibm*2 space group and the *B*-site occupancy of $\frac{3}{4}$ of Al^{3+} in tetrahedral sites and $\frac{1}{4}$ in octahedral sites were considered as previously reported [9,12,13]. In the absence of detectable symmetry changes, all remaining Rietveld refinements were based on the model obtained for the $x = 0$ sample, after suitable compositional adjustments of the occupancy parameters. Fig. 2 shows the experimental and calculated XRD patterns for Ca_2FeAlO_5 and $Mg = 0.05$ (urea route).

For the $x = 0.1$ composition, the refinement was also performed including MgO as a second phase. However, only the most important peak (around 43°) of this MgO phase is distinguishable in the XRD pattern, and no improvement was obtained on the conventional agreement factors. Considering the fact that the refinement of the second phase takes into account just one peak, the exclusion of the 2θ range between 42.30° and 43.50° was preferred.

In order to study the occupancy preference of Mg, several models were considered in the Rietveld refinements of the XRD patterns. A previous study on a doped brownmillerite compound ($Ca_2Fe_{0.95}Al_{0.95}Mg_{0.05}Si_{0.05}O_5$) indicated a preference of Mg^{2+} ions for the octahedral sites [9]. Although slight improvements were obtained in the conventional agreement factors, when considering Mg^{2+} preference for octahedral sites, no conclusion regarding occupancy preferences could be drawn based exclusively on XRD data. The cell parameters values were unaffected by the different site occupancy models and the results obtained, including the conventional agreement factors, are presented in Table 1, as well as some experimental details of the refinements. In Table 2, the estimated atomic positions are presented (only for the compounds prepared by the urea route). In general, it can be noted that the

Table 1
Experimental details and some results obtained by Rietveld refinement of the XRD patterns for the $Ca_2FeAl_{1-x}Mg_xO_5$ compounds

	$x = 0$		$x = 0.05$		$x = 0.10$[a]	
	Urea	Citrate	Urea	Citrate	Urea	Citrate
Interval 2θ (°)	15–120 (for all samples)					
Step	0.02	0.02	0.02	0.02	0.02	0.02
Time/step (s)	10	8	8	8	8	8
I_{max}	31,648	23,654	24,430	20,278	19,488	20,621
N° reflections	200 (for all samples)					
Refinement information						
No. refined parameters	33 (for all samples)					
Excluded regions	In all cases a small region around 30.2° (not identified; relative intensity ≈0.3%)					
	For the $x = 0.10$ composition, a peak between 42.30 and 43.50 identified as MgO					
Lattice parameters and conventional parameters obtained after refinement						
a/Å	5.5639(1)	5.5648(1)	5.5680(1)	5.5675(1)	5.5714(1)	5.5701(1)
b/Å	14.5130(2)	14.5163(3)	14.5328(2)	14.5345(3)	14.5458(3)	14.5410(3)
c/Å	5.3457(1)	5.3451(1)	5.3443(1)	5.3437(1)	5.3482(1)	5.3473(1)
Vol./Å^3	431.66(2)	431.78(2)	432.45(2)	432.42(2)	433.42(2)	433.10(2)
C R_{wp}	9.03	11.1	10.4	11.5	12.8	14.3
C R_p	7.37	8.94	8.62	9.72	10.8	11.7
R_{Bragg}	2.72	2.91	3.81	3.88	5.07	5.86

[a]Not single phase.

Table 2
Refined atomic positions obtained from Rietveld analysis of the XRD data of the compounds obtained by the urea route

	Wyckoff position	Occupancy	x	y	z
Ca_2FeAlO_5					
Ca	8*c*	1	0.0268(2)	0.1084(1)	0.4907(5)
Fe/Al(1)	4*a*	0.75/0.25	0	0	0
Fe/Al (2)	4*b*	0.25/0.75	0.9290(3)	1/4	0.9545(4)
O (1)	8*c*	1	0.2559(6)	0.9882(1)	0.2440(14)
O (2)	8*c*	1	0.0676(4)	0.1444(2)	0.0226(7)
O (3)	4*b*	1	0.8610(7)	1/4	0.6183(8)
$Ca_2FeAl_{0.95}Mg_{0.05}O_5$					
Ca	8*c*	1	0.0266(2)	0.1087(1)	0.4886(5)
Fe/Al/Mg(1)	4*a*	0.75/0.2/0.05	0	0	0
Fe/Al (2)	4*b*	0.25/0.75	0.9295(3)	1/4	0.9543(5)
O (1)	8*c*	1	0.2564(7)	0.9879(2)	0.2407(16)
O (2)	8*c*	1	0.0651(4)	0.1443(2)	0.0220(8)
O (3)	4*b*	1	0.8623(8)	1/4	0.6214(9)
$Ca_2FeAl_{0.9}Mg_{0.1}O_5$					
Ca	8*c*	1	0.0271(2)	0.1086(1)	0.4911(7)
Fe/Al/Mg(1)	4*a*	0.75/0.15/0.1	0	0	0
Fe/Al (2)	4*b*	0.25/0.75	0.9296(4)	1/4	0.9524(6)
O (1)	8*c*	1	0.2544(9)	0.9880(2)	0.2472(21)
O (2)	8*c*	1	0.0691(5)	0.1442(3)	0.0235(10)
O (3)	4*b*	1	0.8587(10)	1/4	0.6232(12)

refinement results are slightly better for compounds prepared by the urea route than for the citrate ones. This result can be related to the fact that the precursor obtained by urea route has already a brownmillerite structure after the thermal treatment at 873 K, contrary to the product obtained by the citrate route. In this case, the formation of some oxides and carbonates can lead to a less-homogeneous product and to some structural defects, undetected by powder XRD. However, the calculated cell parameters values are comparatively almost identical for both routes. Moreover, a slight increase on the cell volume as x increases is observed, in agreement with the higher ion radius of Mg^{2+} in relation to Al^{3+} [14]. The results obtained for the $x = 0$ compound are in agreement with previously published results for the same nominal composition [9,12,13].

The conventional agreement factors obtained on the Rietveld refinements of both $x = 0.1$ samples are significantly

higher than those obtained for the $x = 0$ and 0.05, even excluding the MgO contribution. Other structural models were attempted, namely the *Icmm* space group which has been reported for other brownmillerite structures [15], as a result of tetrahedral disordered arrangement. However, in these attempts, significant differences were observed on the intensity of some reflections, leading to higher values of the conventional agreement factors ($R_{wp} = 15$, $R_p = 10.9$ and $R_{Bragg} = 5.9$). Although different models like intermixed brownmillerite-type phases, modulated structures or other disordered models could be considered, as previously reported for other brownmillerite compounds [7,16,17], neutron diffraction or transmission electron microscopy studies would be necessary for this investigation.

Based on the results of the present work, only the hypothesis of a non-homogeneous phase can be proposed, most probably due to the presence of micro domains with different compositions or to some structural disorder caused by different tetrahedral chain ordering. In fact, it is well known that it is difficult to distinguish between the different variants of ordered structures on brownmillerite compounds and the presence of such disorder causes difficulties on the XRD pattern refinements [17]. This hypothesis is supported by the Mössbauer spectroscopy, magnetisation and electrical results as explained below.

In order to evaluate the effect of magnesium doping on the structure, selected bond lengths and angles are summarised in Table 3, for the $x = 0$ and 0.05 compounds obtained by the urea route. Fig. 3 corresponds to a structural schematic showing two tetrahedra and one octahedron for easier understanding of Table 3. From these results, it can be deduced that the substitution of Al^{3+} by Mg^{2+} did not lead to significant structural modifications, which is coherent with the small amount of doping (0.05). The bond lengths are almost identical, both for octahedron and tetrahedron, and the only significant difference corresponds to a slight increase of the O2–*M*2–O2 angle, which can be taken as a measure of tetrahedral chain deformation induced by the presence of magnesium on the octahedral sites. The significant difference between the equatorial and apical bond lengths of the octahedral site and consequent shorter *M*(2)–O2 bond length is an usual observation on brownmillerite structures.

Table 4 presents the determined Fe^{4+} content for each sample, as obtained by Mohr's salt titration. According to the obtained results, and taking into consideration the associated error, the citrate route led to slightly more oxidised compounds than those obtained using urea. A small fraction of Fe^{4+} was also detected for the $x = 0$ sample prepared by the citrate route, as reported for a sample with the same nominal composition prepared by a glycine–nitrate process [18]. However, no Fe^{4+} was found for the same composition obtained by the urea route in this work. Although a Fe^{4+} value identical to the amount of the performed substitution was obtained for the $x = 0.05$ samples, an unexpected decrease on the Fe^{4+} content is observed for the $x = 0.1$ samples. This result can be explained by the presence of MgO impurity as detected by XRD.

Table 3
Selected bond lengths (Å) and angles (°) for the $x = 0$ and $x = 0.05$ compounds obtained by urea route

	$x = 0$	$x = 0.05$
Octahedral bond lengths (Å)		
M(1)–O1 (2*x*)	1.938(6)	1.930(6)
M(1)–O1 (2*x*)	1.936(6)	1.947(7)
M(1)–O2 (2*x*)	2.133(3)	2.132(3)
⟨M(1)–O⟩	*2.002*	*2.003*
Tetrahedral bond lengths (Å)		
M(2)–O2 (2*x*)	1.753(2)	1.749(3)
M(2)–O3	1.837(5)	1.818(5)
M(2)–O3	1.835(4)	1.854(5)
⟨M(2)–O⟩	*1.7945*	*1.7925*
Octahedral angles (°)		
O1–M1–O1	95.4(3)	96.4(4)
	87.3(5)	87.3(6)
	177.3(5)	176.8(7)
	90.0(3)	89.5(4)
O1–M1–O2	85.4(3)	85.8(3)
	90.3(3)	90.0(3)
	90.2(3)	90.5(3)
	94.4(3)	94.0(3)
Mean value	*90.075*	*90.075*
O2–M1–O2	173.5(2)	173.7(2)
Tetrahedral angles (°)		
O2–M2–O2	121.8(2)	122.8(3)
O2–M2–O3	107.1(3)	106.9(3)
	106.7(3)	106.2(3)
O3–M2–O3	106.6(3)	106.9(4)

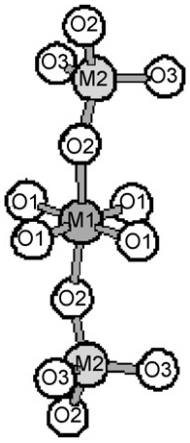

Fig. 3. Schematic representation of the Ca_2FeAlO_5 structure showing two tetrahedra and one octahedron.

3.2. Mössbauer spectroscopy

The performed studies show no direct dependency of the obtained spectra on the preparation method. The spectra

Table 4
Fe^{4+} content as determined by titration, with an estimated error on Fe^{4+} of approximately 0.01

	Fe^{4+} content $Ca_2FeAl_{1-x}Mg_xO_5$	
x	Urea route	Citrate route
0	0	0.01
0.05	0.04	0.05
0.10[a]	0.03	0.04

[a]Not single phase.

of the compounds prepared by the urea route and obtained at 4 K are presented in Fig. 4. These spectra are similar to those reported for a Ca_2FeAlO_5 phase [18–20] and were fitted as explained in Ref. [18]. They clearly show two magnetic sextets, one assigned to octahedral and the other to tetrahedral Fe^{3+}. The site ratio found is in agreement with the occupancy used in the Rietveld refinements. Estimated parameters are summarised in Table 5, which also includes the citrate route obtained phases. For the Mg-containing samples, small absorption peaks are detected at about −2 mm/s in the corresponding spectra (Fig. 4), but in the Ca_2FeAlO_5 spectra there is no evidence of such absorption peak. Accordingly, a third sextet was fitted in the former spectra, with parameters typical of Fe^{4+}, while attempts to do the same for Ca_2FeAlO_5 consistently lead to worse agreement factors than the simpler two-sextet fit. This means that, in agreement with Mohr's salt titration of the sample prepared by the urea route (see Table 4), no Fe^{4+} is detected for the $x = 0$ compound by Mössbauer spectroscopy. In the case of Ca_2FeAlO_5 prepared by the citrate route, titration data indicate the presence of 0.01 Fe^{4+} per f.u., a value which is within the experimental error for these data. On the other hand, this small Fe^{4+} content may be below the detection limit of the present Mössbauer measurements, justifying the difficulty to observe such a small value by this technique. Assuming similar recoilless factors for Fe^{4+} and for Fe^{3+} in both coordinations [18,21], the concentration of Fe^{4+} cations deduced from Mössbauer data in the Mg-containing samples is equal to the estimated relative areas (Table 5). Considering the estimated standard deviations, the Fe^{4+} contents are in good agreement with the titration (Table 4).

At 297 K, and except for both $Ca_2FeAl_{0.95}Mg_{0.05}O_5$ samples, all the spectra show broad unresolved peaks due to the proximity of the magnetic ordering transition (Fig. 5). This fact made the extraction of accurate information impossible to obtain, as previously reported for a $x = 0$ sample [18].

Based on the magnetisation results shown below, Mössbauer measurements of the $x = 0$ and 0.10 samples prepared by the urea route were performed at 363 and 353 K, respectively. The fit of these two spectra as well as the room-temperature spectra of the $x = 0.05$ sample may

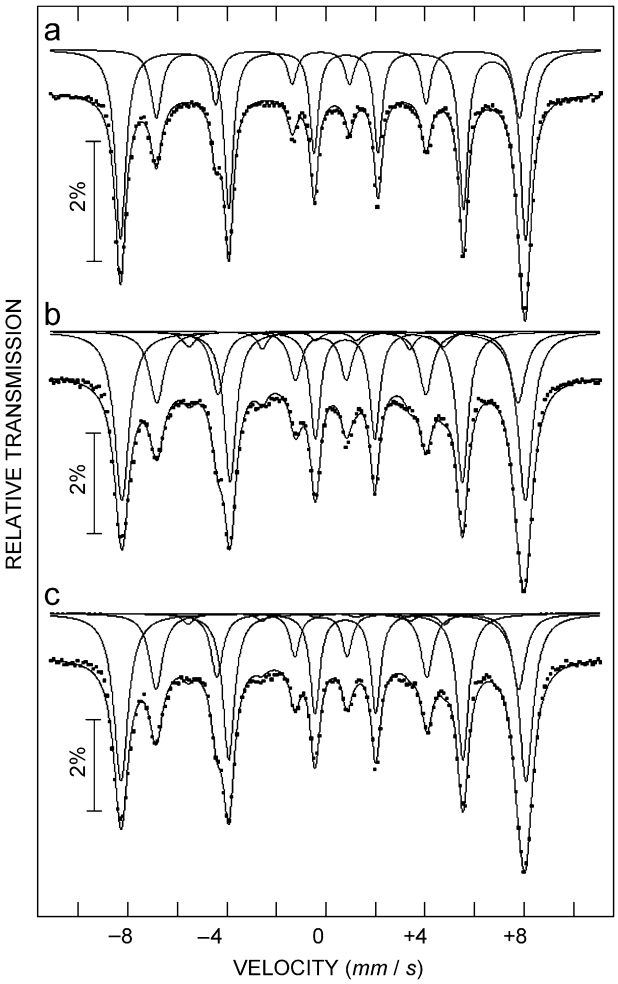

Fig. 4. Mössbauer spectra of the $Ca_2FeAl_{1-x}Mg_xO_5$ compounds obtained by the urea route taken at 4 K. (a) $x = 0.0$; (b) $x = 0.05$; (c) $x = 0.1$.

be properly analysed by quadrupole doublets as presented in Fig. 6, in agreement with magnetisation data which shows that the magnetic ordering of these compounds takes place around 340 and 330 K for the $x = 0$ and 0.1 compositions respectively, but below room temperature for the $x = 0.05$ phase. Very good fittings (Fig. 6 and summary of results in Table 5), are obtained considering either two, for Ca_2FeAlO_5, or three, for Mg-containing samples, doublets with relative areas and hyperfine parameters fully consistent with those estimated for the 4 K spectra of the same samples (Table 5). This confirms the model used to analyse the Mössbauer spectra and the assumption that recoilless factors for Fe^{4+} and for Fe^{3+} are very similar, regardless of coordination.

Both $Ca_2FeAl_{0.90}Mg_{0.10}O_5$ samples show a lower Fe^{4+} content than $Ca_2FeAl_{0.95}Mg_{0.05}O_5$ in agreement with titration data. This may be related to the fact that the $x = 0.10$ samples are not single phase and the obtained brownmillerite phases are most probably not homogeneous. In fact, the room-temperature Mössbauer spectra (Fig. 5) of the $x = 0.1$ composition can be explained by the addition of a paramagnetic spectra with a spectra similar to

Table 5
Parameters estimated from the spectra taken at different temperatures, assigned to Fe oxidation state and coordination

Sample	T (K)	IS (mm/s)	QS, ε (mm/s)	B_{hf} (T)	Γ (mm/s)	I (%)	
Urea route							
Ca_2FeAlO_5	363	0.31	1.62	—	0.35	73	Fe^{3+} oct
		0.11	1.55	—	0.26	27	Fe^{3+} tet
	50	0.46	−0.94	48.7	0.42	73	Fe^{3+} oct
		0.22	0.56	43.1	0.50	27	Fe^{3+} tet
$Ca_2FeAl_{0.95}Mg_{0.05}O_5$	297	0.31	1.55	—	0.38	66	Fe^{3+} oct
		0.12	1.50	—	0.30	30	Fe^{3+} tet
		0.02	1.34	—	0.34	4	Fe^{4+}
	4	0.47	−0.90	50.5	0.53	66	Fe^{3+} oct
		0.25	0.63	45.2	0.59	30	Fe^{3+} tet
		0.14	−0.70	31.7	0.50	4	Fe^{4+}
$Ca_2FeAl_{0.9}Mg_{0.1}O_5$ (not single phase)	353	0.31	1.56	—	0.35	65	Fe^{3+} oct
		0.12	1.50	—	0.27	32	Fe^{3+} tet
		−0.01	1.22	—	0.36	3	Fe^{4+}
	4	0.48	−0.91	50.7	0.55	68	Fe^{3+} oct
		0.26	0.63	45.4	0.54	29	Fe^{3+} tet
		0.14	−0.78	32.1	0.50	3	Fe^{4+}
Citrate route							
Ca_2FeAlO_5	50	0.46	−0.94	48.4	0.43	73	Fe^{3+} oct
		0.20	0.55	43.1	0.49	27	Fe^{3+} tet
$Ca_2FeAl_{0.95}Mg_{0.05}O_5$	297	0.31	1.59	—	0.36	65	Fe^{3+} oct
		0.12	1.53	—	0.28	30	Fe^{3+} tet
		0.02	1.47	—	0.28	6	Fe^{4+}
	4	0.47	−0.90	50.4	0.57	65	Fe^{3+} oct
		0.27	0.69	45.3	0.73	30	Fe^{3+} tet
		0.13	−0.80	32.1	0.49	6	Fe^{4+}
$Ca_2FeAl_{0.9}Mg_{0.1}O_5$ (not single phase)	4	0.47	−0.89	50.7	0.52	68	Fe^{3+} oct
		0.26	0.65	45.4	0.55	29	Fe^{3+} tet
		0.14	−0.80	31.9	0.53	3	Fe^{4+}

IS—isomer shift relative to metallic α-Fe at 297 K. QS—quadrupole splitting for a doublet. $\varepsilon = (e^2V_{ZZ}Q/4)\,(3\cos^2\theta—1)$—quadrupole shift for magnetic sextets. Γ—line-widths. B_{hf}—magnetic hyperfine field. Estimated errors are <1% for I, ⩽0.2 T for B_{hf} and ⩽0.02 mm/s for IS, QS, ε, and Γ.

the one obtained for the $x = 0$ compound. Formation of MgO further indicates that the global Mg content in the brownmillerite phases is lower than 0.10 per f.u.

Although the differences between the relative areas of Fe^{3+} in tetrahedral coordination found in Ca_2FeAlO_5 and in the Mg-containing samples are within the experimental error, the most probable values of these parameters (Table 5) are systematically higher in the latter samples. This may suggest that there is a preference for octahedral coordination of Mg^{2+} relative to Fe^{3+}, even assuming that all the Fe^{4+} is in octahedral coordination. These results corroborate the tendency found during the Rietveld refinements of the XRD patterns and are in agreement with reported results on a Mg-containing brownmillerite compound [9].

3.3. Magnetisation measurements

Fig. 7A shows the magnetisation versus temperature curves for the $x = 0$ and 0.05 compounds (prepared by the urea route) collected at 0.05 T, after zero-field cooling (ZFC) and field cooling (FC), and Fig. 7B represents the inverse susceptibility plot, where the results obtained for the $x = 0.10$ composition are also included. A small irreversibility is detectable at low temperatures and a small but significant kink is observed around 340 and 290 K for the $x = 0$ and 0.05 compounds, respectively. In the case of $x = 0.10$, an almost undetectable kink can be noticed around 330 K, as indicated on the inverse susceptibility plot (Fig. 7B).

From the cross data of these results and Mössbauer spectra, it can be deduced that the temperatures at which the kinks are observed, 340 and 290 K, correspond to the magnetic ordering temperature of the $x = 0$ and 0.05 compositions, respectively. This interpretation is corroborated by the magnetisation versus applied magnetic field curves collected at different temperatures, as exemplified for the $x = 0.05$ compound in Fig. 8. The straight lines represent linear fits to the first 10 points (low fields) of each curve. The fit reproduces all data for temperatures above the kink temperature value ($T = 330$ K curve), showing that, only for those temperatures, the $x = 0.05$ sample is in a complete paramagnetic state. Below the ordering temperature, the overall magnetic behaviour is antiferromagnetic, with the iron cations as sole contributors to the exchange interactions. The magnetic loop displayed in the inset of Fig. 7A for the $x = 0.05$ sample illustrates the weak coercivity displayed by this compound

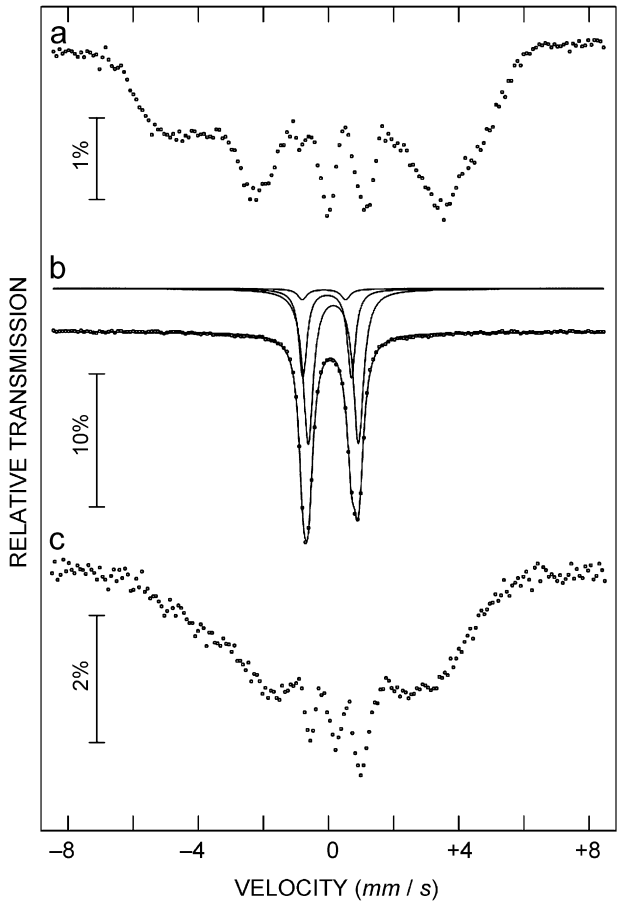

Fig. 5. Room-temperature Mössbauer spectra of the $Ca_2FeAl_{1-x}Mg_xO_5$ compounds obtained by the urea route (a) $x = 0.0$; (b) $x = 0.05$; and (c) $x = 0.1$.

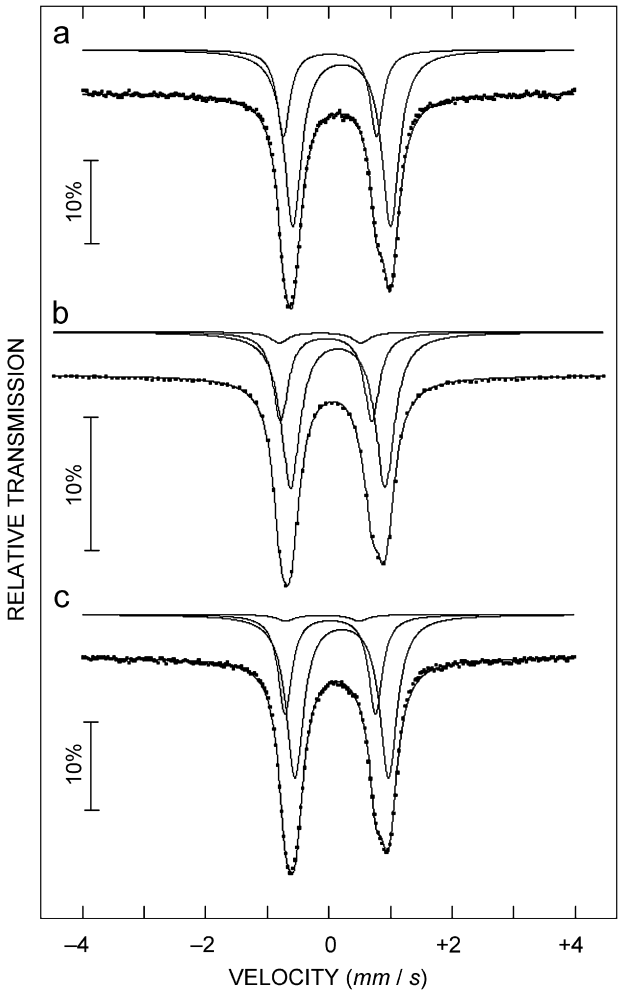

Fig. 6. Mössbauer spectra of the $Ca_2FeAl_{1-x}Mg_xO_5$ compounds obtained by the urea route. (a) $x = 0.0$, $T = 363$ K; (b) $x = 0.05$, $T = 297$ K; and (c) $x = 0.1$, $T = 353$ K.

and shows that no important ferromagnetic component was present.

From the inverse susceptibility plotted in Fig. 7B, it is clear that the sample with $x = 0.05$ has a magnetic behaviour very similar to the non-doped sample, although displaying a lower temperature transition, whereas the $x = 0.1$ compound shows a different magnetic behaviour. In this case, the non-homogeneity of the compound should correspond to the existence of regions with different degrees of Mg doping, implying a less drastic effect of the Mg in breaking the long-range antiferromagnetic interaction among the iron ions. For this sample, the kink in the magnetisation curve is less clear and cannot be attributed to the temperature ordering of a well-defined phase, although, according to the Mössbauer results, the whole sample is in a paramagnetic state above 330 K.

The $M(T)$ curves of both $x = 0$ and 0.05 compounds, show a net increase of the susceptibility with decreasing temperature. Since the Mössbauer results at 4.2 K undoubtedly show that there are no paramagnetic contributions from the iron cations, and since all other ions in the compound contribute diamagnetically, such increase cannot be assigned to a superimposed paramagnetic component. From the low temperature Mössbauer and $M(H)$ data it can be assumed that, at such temperatures, all iron cations in both octahedral and tetrahedral sites are antiferromagnetically ordered. The magnetisation decrease with increasing temperature corresponds to a weakening of the magnetic interactions and can be associated with different spin relaxations of the iron cations depending on their different environments, probably occurring faster for those on tetrahedral sites. The ordering temperature detected around 340 and 290 K for the $x = 0$ and 0.05 compounds, respectively, may be related with stronger antiferromagnetic interactions between iron cations in nearest neighbour octahedral positions within the octahedral plans.

Finally, a magnetisation enhancement with the introduction of Mg is observed, in accordance with the higher hyperfine field found by Mössbauer spectroscopy for the $x = 0.05$ compound (Table 5). Taking into account that the magnetisation of both compounds at the highest temperatures is similar (see Fig. 7) and that Fe^{4+} magnetic moment is lower than Fe^{3+}, the observed change should be essentially due to the distribution of iron cations among

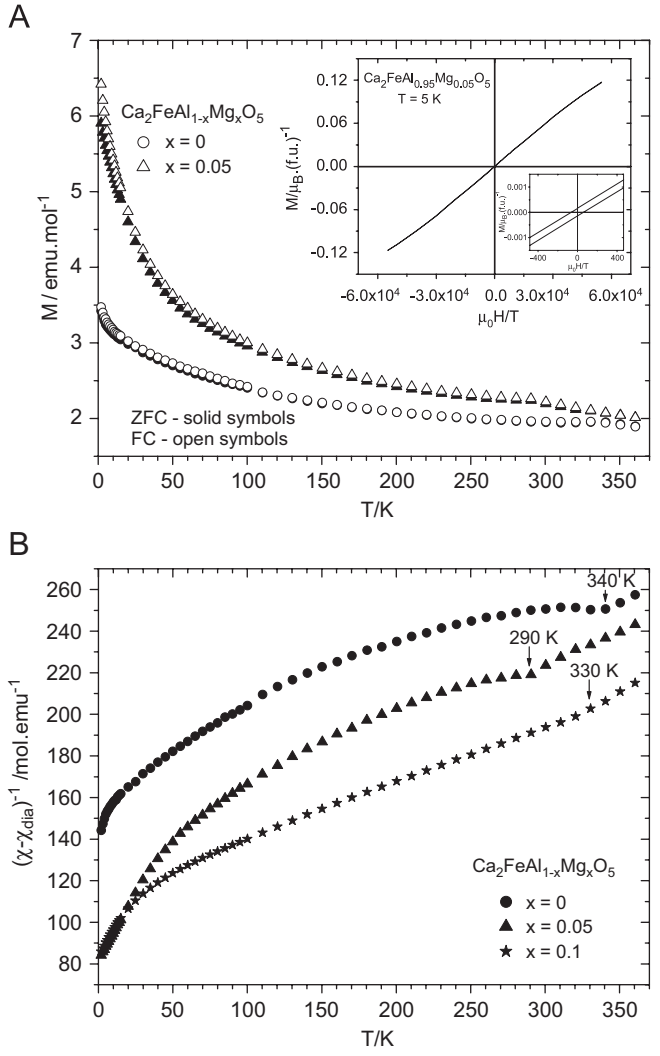

Fig. 7. (A) Temperature dependence of the ZFC-FC magnetisation measured under 50 mT for $x = 0$ and 0.05 compounds. The inset shows the hysteresis curve collected at 5 K. (B) Inverse of the magnetic susceptibility (diamagnetic component subtracted) as a function of the temperature for $x = 0$, 0.05 and 0.1.

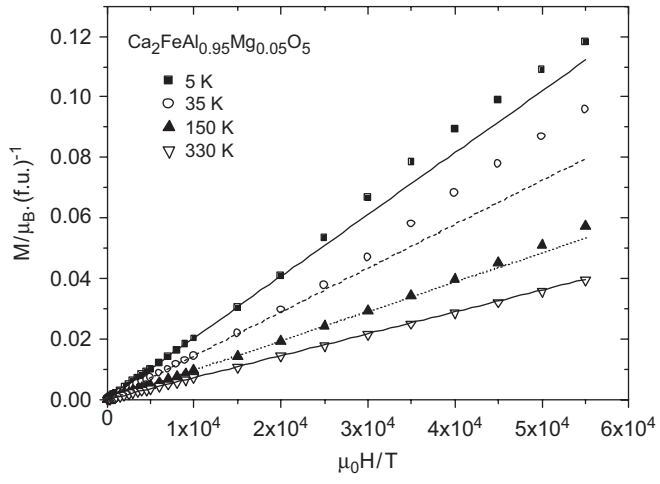

Fig. 8. Magnetisation versus applied magnetic field collected at different temperatures. The depicted lines are visual aids.

Table 6
Activation energies for electrical conduction, E_a, obtained from fitting the Arrhenius equation $\sigma = (\sigma_0/T)\exp(-E_a/kT)$ to the experimental data

	E_a (eV)	
	Region 1 (873–556 K)	Region 2 (<556 K)
$Ca_2FeAl_{1-x}Mg_xO_5$ (urea)		
$x = 0.00$	0.45(1)	0.62(1)
$x = 0.05$	0.26(1)	0.34(1)
$x = 0.10$[a]	0.28(1)	0.37(1)
$Ca_2FeAl_{1-x}Mg_xO_5$ (citrate)		
$x = 0.00$	0.31(1)	0.38(1)
$x = 0.05$	0.26(1)	0.34(1)
$x = 0.10$[a]	0.27(1)	0.36(1)

[a]Not single phase.

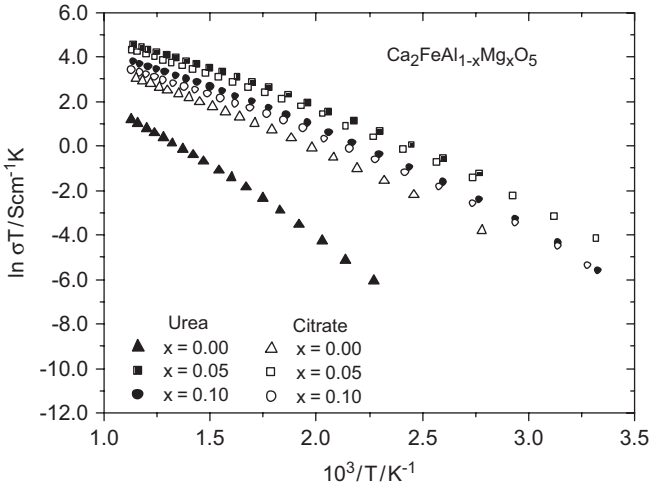

Fig. 9. Arrhenius plot of the total electrical conductivity, in air, for samples $Ca_2FeAl_{1-x}Mg_xO_5$ with $x = 0$, 0.05 and 0.1 prepared by both urea/nitrate and citrate routes.

the octahedral and tetrahedral sites. Structural and Mössbauer results suggest a preference of the Mg ions for the octahedral sites. Moreover, Mössbauer results for the $x = 0.05$ sample are consistent with an increase of iron cations in tetrahedral coordination, in comparison to the Ca_2FeAlO_5 compound. Thus, it seems that the magnetic enhancement below the transition temperature must be related to the coupling between octahedral iron cations of different octahedral planes, due to the increased number of the latter on tetrahedral sites.

3.4. SEM and electrical behaviour

Fig. 9 shows the Arrhenius plots of the total electrical conductivities for $Ca_2FeAl_{1-x}Mg_xO_5$ ($x = 0$, 0.05 and 0.1) samples, prepared by both methods. The electrical conductivity, in air, of each composition increases with increasing temperature in the full studied range, varying from 3×10^{-3} S/cm ($x = 0$) up to 0.1 S/cm (Mg = 0.05) at about 873 K. The global results indicate a close relation

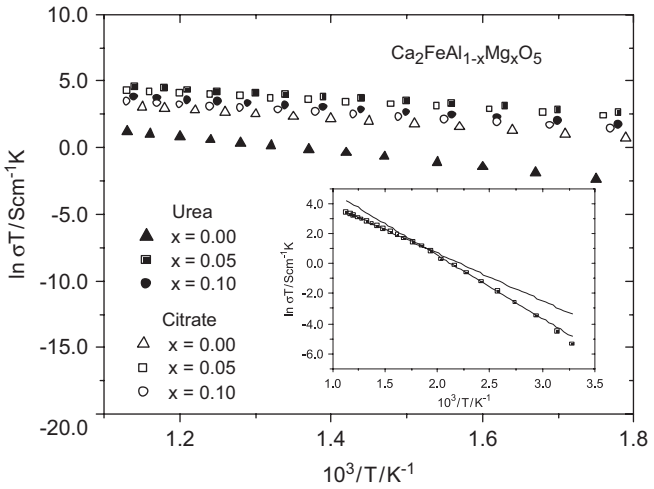

Fig. 10. High-temperature region Arrhenius plot of the total electrical conductivity, in air, for samples $Ca_2FeAl_{1-x}Mg_xO_5$ with $x = 0$, 0.05 and 0.1 (both routes). The inset shows the Arrhenius plot of the total electrical conductivity for sample with nominal composition $Ca_2FeAl_{0.95}Mg_{0.05}O_5$ (urea), exemplifying the two distinct regions of thermally activated small polaron hopping type conduction.

between Fe^{4+} and conductivity performance of the prepared compounds, with the $x = 0.05$ compositions presenting the highest conductivities. For the $x = 0$ compound, a significant difference on the conductivity can be observed when both preparation methods are compared, contrary to the other samples for which very similar results are found. The better conductivity of the Ca_2FeAlO_5 compound obtained by the citrate route can be related to the indication that some Fe^{4+} can be present on this compound, as determined by titration. However, the quantity of detected Fe^{4+} is too small to account for the observed increase in electrical conductivity for both $x = 0$ samples. Therefore, the microstructural influence cannot be disregarded.

A small degradation on the conductivity performance from $Mg = 0.05$ to 0.1 can be observed, which, again, is consistent with the fact that the $x = 0.10$ composition does not, as previously mentioned, correspond to a pure phase.

The samples exhibit an almost linear behaviour of $\ln(\sigma T)$ versus $1/T$ in the full studied temperature range, a relationship which is usually attributed to an adiabatic

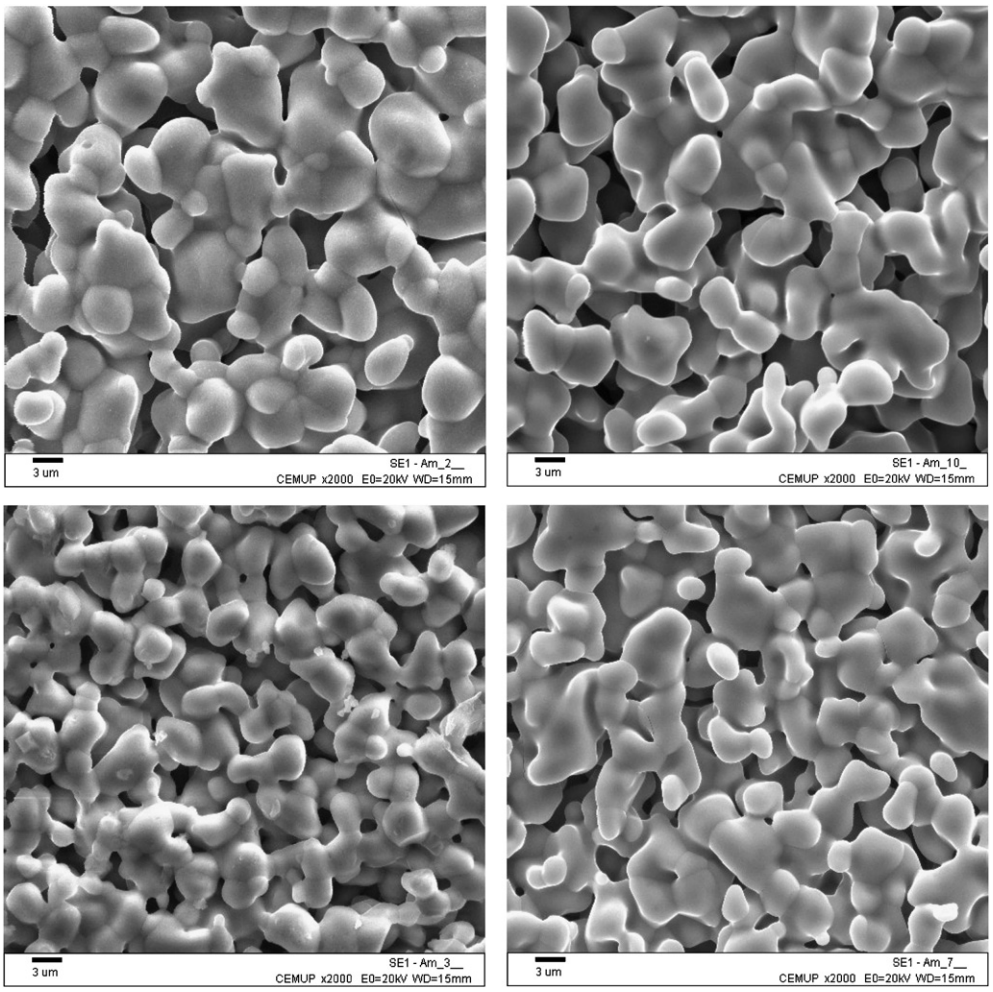

Fig. 11. SEM images exemplifying the microstructure of the pellets used in the electrical conductivity measurements with nominal compositions $Ca_2FeAl_{1-x}Mg_xO_5$ ($x = 0$ and 0.05, left and right images, respectively) by citrate route (upper figure) and urea route (lower figure).

small-polaron hopping mechanism [22,23]. However, improved linear fits were obtained when two distinct regions were considered, one at temperatures ranging from ~873 to ~573 K (region 1) and another at temperatures below ~573 K (region 2). The existence of two linear regimes, with slightly different activation energy values is probably related to changes in the number of carriers and/or their mobility with temperature. The activation energies for conduction, E_a, were determined from the gradient of the Arrhenius plots in the two temperature regions and are presented in Table 6. For easier comparison between samples, Fig. 10 plots $\ln(\sigma T)$ vs. $1/T$ for region 1 and the inset exemplifies the fitting performed on both temperature regions for a $Ca_2FeAl_{0.95}Mg_{0.05}O_5$ compound. The E_a for the undoped sample is in good agreement, although slightly lower, with that obtained by Kharton et al. [12] for a sample with the same nominal composition.

The differences in E_a between the two regions are more significant for the Ca_2FeAlO_5 compound than for the Mg-doped samples and, again, the $x = 0$ sample prepared by citrate route exhibiting a smaller activation energy value than the one prepared using urea. A decrease in E_a is observed from $x = 0$ to 0.05 compounds, in both regions and for both preparation methods. In region 1, corresponding to the highest temperatures, the activation energy for conduction decreases from ~0.45 eV (urea) or ~0.31 eV (citrate), which is the case for $x = 0$, to a minimum of ~0.26 eV for the Mg = 0.05 samples, which is consistent with increased density of charge carriers. Nevertheless, the activation energies are relatively high for all studied compositions and could be associated to reduced hopping frequency.

The morphology of the pellets used in the electrical conductivity measurements was investigated by SEM. Fig. 11 presents SEM images of Ca_2FeAlO_5 and $Ca_2FeAl_{0.95}Mg_{0.05}O_5$ prepared by both the citrate and urea routes. Except for the $x = 0$ sample prepared by the citrate route, no significant morphological differences were found between the compounds.

From these results, the global improvement observed on the electrical conductivity of the $x = 0.05$ samples is most probably due to differences on the number or mobility of the charge carriers, for which Fe^{4+} has an important role. However, the differences observed on the electrical properties of the Ca_2FeAlO_5 phase seem to be associated not only to the presence of some Fe^{4+} (0.01) on the sample prepared by the citrate method, but also to the influence of a slightly larger grain size for this particular sample.

4. Conclusions

$Ca_2FeAl_{1-x}Mg_xO_5$ ($x = 0$, 0.05 and 0.1) compounds with the brownmillerite structure were prepared and characterised by XRD, SEM, Mössbauer spectroscopy, magnetisation and electrical measurements. Pure phases were obtained for $x = 0$ and 0.05, but the magnesium solubility limit was reached for $x = 0.1$, where the presence of non-homogeneous phases explains the results obtained by different techniques. The comparison of the XRD evolution during the synthesis allows to conclude that the brownmillerite structure is easier to obtain using urea rather than citrate as fuel. Although high temperature treatments (around 1550 K) were used in this work, the results suggest that other brownmillerite compounds could be prepared at lower temperatures using this urea route.

Mohr's salt titrations and Mössbauer measurements show that Mg doping leads to the oxidation of some Fe^{3+} and subsequent enhancement of the electrical conductivity. Magnetisation data allow to conclude that Mg doping weakened the antiferromagnetic exchange interactions between iron cations (higher ordering temperature for the non-doped compounds), but increases the magnetisation at low temperatures. This last result is explained in terms of the increased number of iron cations in tetrahedral sites (since XRD and Mössbauer data are consistent with a Mg^{2+} preference for octahedral sites), inducing the magnetic coupling between octahedral iron cations in different octahedral planes.

The compounds exhibit a semiconductor behaviour, with temperature dependences normally attributed to a small polaron hopping conduction mechanism. Although the overall conductivity is lower than that required for the envisaged applications, light doping with Mg was proven to be a suitable way of improving the total electrical conductivity, with no detrimental effects on structure.

Acknowledgments

T. Ramos acknowledges FCT, Portugal, for the post-doctoral grant SFRH/BPD/14028/2003. The authors are grateful to Dr. Carlos M. Sá from the Centro de Materiais da Universidade do Porto, for the SEM images. This work was supported by FCT, POCI, and co-financed by FEDER (POCI/QUI/58915/2004).

References

[1] C.N.R. Rao, Mater. Sci. Eng. B 18 (1993) 1–21.
[2] S.Ya. Istomin, S.V. Abdyusheva, G. Svensson, E.V. Antipov, J. Solid State Chem. 177 (2004) 4251–4257.
[3] M. Kakihana, M. Arima, M. Yoshimura, N. Ikeda, Y. Sugitani, J. Alloys Comp. 283 (1999) 102–105.
[4] K.C. Patil, S.T. Aruna, T. Mimani, Curr. Opin. Solid State Mater. Sci. 6 (2002) 507–512.
[5] F. Lindberg, G. Svensson, S.Ya. Istomin, S.V. Aleshinskaya, E.V. Antipov, J. Solid State Chem. 177 (2004) 1592–1597.
[6] P. Berastegui, S.G. Eriksson, S. Hull, Mat. Res. Bull. 34 (1999) 303–314.
[7] A.M. Abakumov, M.G. Rozova, B.Ph. Pavlyuk, M.V. Lobanov, E.V. Antipov, O.I. Lebedev, G. van Tendeloo, D.V. Sheptyakov, A.M. Balagurov, F. Bourée, J. Solid State Chem. 158 (2001) 100–111.
[8] M. Schwartz, J.H. White, A.F. Sammels, US Patent 6 033 632, 2000.
[9] A.C. Jupe, J.K. Cockcroft, P. Barnes, S.L. Colston, G. Sankar, C. Hall, J. Appl. Crystallogr. 34 (2001) 55–61.
[10] T. Roisnel; J. Rodriguez-Carvajal, FullProf Suite, April 2005.
[11] J.C. Waerenborgh, M.O. Figueiredo, J.M.P. Cabral, L.C.J. Pereira, Phys. Chem. Min. 21 (1994) 460–468.

[12] V.V. Kharton, I.P. Marozau, N.P. Vyshatko, A.L. Shaula, A.P. Viskup, E.N. Naumovich, F.M.B. Marques, Mater. Res. Bull. 38 (2003) 773–782.
[13] A.A. Colville, S. Geller, Acta Crystallogr. B 27 (1971) 2311–2315.
[14] R.D. Shannon, Acta Crystallogr. A 32 (1976) 751–767.
[15] F. Lindberg, S.Ya. Istomin, P. Berastegui, G. Svensson, S.M. Kazakov, E.V. Antipov, J. Solid State Chem. 173 (2003) 395–406.
[16] S. Lambert, H. Leligny, D. Grebille, D. Pelloquin, B. Raveau, Chem. Mater. 14 (2002) 1818–1826.
[17] A.M. Abakumov, A.S. Kalyuzhnaya, M.G. Rozova, E.V. Antipov, J. Hadermann, G. Van Tendeloo, Solid State Sci. 7 (2005) 801–811.
[18] J.C. Waerenborgh, D.P. Rojas, N.P. Vyshatko, A.L. Shaula, V.V. Kharton, I.P. Marozau, E.N. Naumovich, Mater. Lett. 57 (2003) 4388–4393.
[19] R.W. Grant, J. Chem. Phys. 51 (1969) 1156–1162.
[20] R.W. Grant, S. Geller, H. Wiedersich, U. Gonser, L.D. Fullmar, J. Appl. Phys. 39 (1968) 1122–1123.
[21] J.C. Waerenborgh, F.M. Figueiredo, J.R. Frade, M.T. Colomer, J.R. Jurado, J. Phys. Condens. Mat. 13 (2001) 8171–8187.
[22] D.P. Karim, A.T. Aldred, Phys. Rev. B 20 (1979) 2255–2263.
[23] L.W. Tai, M.M. Nasrallah, H.U. Anderson, D.M. Sparlin, S.R. Sehlin, Solid State Ionics 76 (1995) 259–271.